Hindawi
Journal of Robotics
Volume 2023, Article ID 9896453, 1 page
https://doi.org/10.1155/2023/9896453

Retraction

Retracted: Multiscale Motion Detection and Recognition Combining Still Images and Video Sequences

Journal of Robotics

Received 8 August 2023; Accepted 8 August 2023; Published 9 August 2023

This article has been retracted by Hindawi following an investigation undertaken by the publisher [1]. This investigation has uncovered evidence of one or more of the following indicators of systematic manipulation of the publication process:

(1) Discrepancies in scope
(2) Discrepancies in the description of the research reported
(3) Discrepancies between the availability of data and the research described
(4) Inappropriate citations
(5) Incoherent, meaningless and/or irrelevant content included in the article
(6) Peer-review manipulation

The presence of these indicators undermines our confidence in the integrity of the article's content and we cannot, therefore, vouch for its reliability. Please note that this notice is intended solely to alert readers that the content of this article is unreliable. We have not investigated whether authors were aware of or involved in the systematic manipulation of the publication process.

Wiley and Hindawi regrets that the usual quality checks did not identify these issues before publication and have since put additional measures in place to safeguard research integrity.

We wish to credit our own Research Integrity and Research Publishing teams and anonymous and named external researchers and research integrity experts for contributing to this investigation.

The corresponding author, as the representative of all authors, has been given the opportunity to register their agreement or disagreement to this retraction. We have kept a record of any response received.

References

[1] Z. Chen, "Multiscale Motion Detection and Recognition Combining Still Images and Video Sequences," *Journal of Robotics*, vol. 2022, Article ID 7682559, 12 pages, 2022.

Hindawi
Journal of Robotics
Volume 2022, Article ID 7682559, 12 pages
https://doi.org/10.1155/2022/7682559

Research Article

Multiscale Motion Detection and Recognition Combining Still Images and Video Sequences

Zhuo Chen

College of Information Engineering, Xinyang Agriculture and Forestry University, Xinyang 464000, Henan, China

Correspondence should be addressed to Zhuo Chen; 2014270001@xyafu.edu.cn

Received 13 July 2022; Revised 28 July 2022; Accepted 6 August 2022; Published 31 August 2022

Academic Editor: Shahid Hussain

In order to improve the sports training and competition effect of sports, this paper combines the accurate recognition method of video image fuzzy features to accurately identify the sports process to explore the movement characteristics of athletes on the sports stage. Moreover, this paper uses the trigger system to select cases and adopts the all-digital trigger method in the digital sports video recognition system. In addition, this paper uses the ADC input overrange as the judgment standard for bad cases and constructs an accurate recognition system for sports training features based on video image recognition. Finally, this paper verifies the effect of the accurate recognition method of local fuzzy features in sports video images. The experimental study verifies the effectiveness of the accurate recognition method of local fuzzy features in sports video images.

1. Introduction

At present, in physical training, strength training and speed training are the two major focuses. Explosive strength training is mainly used in athletes' starting and sports training stages, while speed training is mainly used in athletes accelerating and maintaining high speed. Moreover, athletes with good explosiveness and speed can achieve good results in sports training. In addition, explosive power and speed are important sports qualities that sports athletes need to have, and they are also the basis for athletes to successfully learn other sports and skills and have a significant impact on sports performance.

Explosive power means that the athlete changes from a static state to a moving state in the shortest time during the starting process, and the body obtains the maximum forward momentum, creating favorable conditions for the acceleration process in the running phase [1]. The training of explosive power is very important for sports training. To a certain extent, the strength of explosive power determines the starting speed of the athlete. A fast starting speed lays the foundation for the subsequent acceleration process of the athlete. The acceleration link catches up with the opponent and restores the distance. During the competition, an athlete with a slow start and weak explosiveness is undoubtedly not an excellent athlete [2]. From the point of view of explosive power, this not only represents the speed of the athlete's reaction but also shows the problems existing in the athlete's explosive power training, and the physical quality is not as good as the athlete with strong explosive power. The physical quality, strength, and speed also determine the ability of the athlete. Only by enhancing the explosive power and improving the starting speed of the athlete can we get a good start at the beginning of the competition [3]. Practice has proved that the use of fast single-leg jumping exercises has a very significant effect on improving the strength of the lower limbs of sports trainees [4].

The Role of Hopping Exercises in Developing Effective Muscle Groups for Sports Trainees. When an athlete is exercising, most of the muscles in the body begin to work, and different training programs exercise different muscle groups. During training, sports trainees will use the iliopsoas, quadriceps, triceps calf, posterior calf muscles, and ankle joints. Improving the strength of these muscle groups is a guarantee for sports trainees to carry out targeted training in the future. *The Key to Exercising Effective Muscle Groups* [5]. In daily training, it is easy to ignore the muscles on the back of the athlete's calf, but in the process of running, the

hamstrings play a back-push. If this part of the muscle group is not fully exercised, resulting in insufficient development of this muscle group, it is easy to cause muscle strain on the back of the thigh [6]. The athlete's quadriceps and iliopsoas mainly help the athlete to ensure that the body does not lean back when raising the thigh. The exercise of the ankle joint can ensure that the athlete can push back smoothly and quickly place the center of gravity in the front [7].

One-Legged Hopping Training during the Starting Process. In the process of sports training, athletes usually use the squatting starting position when starting. This starting position can help athletes start quickly and can analyze the rapid single-legged hopping in sports teaching in a short time (training [8]).

The starting process mainly uses the explosive power of the body to quickly get rid of the static state, so as to achieve the fastest initial speed and lay the foundation for the athlete's subsequent accelerated running. We know that in the process of starting, athletes need to have great strength and explosive power in their lower limbs. The explosive power of lower limbs is a prerequisite for determining the starting speed of athletes, and strength is the guarantee for athletes to accelerate during running. After the sound of gunshots, the athlete should push back quickly to push the body forward, swing his arms greatly, and move the body forward rapidly [9]. In the process of training, coaches can take single-leg jump training to strengthen students' strength and lower body explosiveness. According to the physical fitness of the athlete, they formulate training methods that meet the physical condition of the athlete. For example, let the athletes perform single-leg squat exercises rhythmically, with 6–8 squatting as a group, and repeat 3–5 groups. During the training process, certain adjustments can be made according to the athlete's exercise level and physical tolerance and appropriately increase some weights to train the athlete's lower body strength. In the process of training, the training focus should be placed on effective muscle groups, the weight should be reasonably arranged, the weight should be adjusted appropriately according to the actual situation of the athlete, and the lower limb strength and explosive training of the athlete should be strengthened, so that the athlete can occupy the opportunity [10].

Hop Training in Acceleration Running. Acceleration running is the stage in which the athlete rushes out of the starting line and before the midway run after the athlete starts. Generally, the distance of accelerated running is 25–30 meters. Men usually use 13–15 steps to complete the accelerated run, and women usually use 15–17 steps to complete. Through observation, we can find that at the initial number of steps at the start, the landing points of the athlete's legs are two parallel lines with the same distance (straight line [11]). In the stage of accelerated running, if the stride length changes, under the same stride frequency, the increase of the stride length will accelerate the increase of the speed, and the decrease of the step length will lead to the decrease of the speed. The process of accelerated running is to make efficient use of the athlete's explosive power and give full play to the strength of the body in the accelerated running phase to achieve maximum speed. In the process of accelerated running, the athlete's lower body explosive power and physical tolerance play a key role, so coaches should strengthen the training of these two aspects of the athlete in the training process. Rapid hopping is a very efficient training method [12]. When training single-leg hopping, athletes use two methods of single-leg jumping and 20-meter single-leg jumping training. When jumping with one leg to reach a height, the athlete should jump up immediately after landing on one leg, switch feet for 15 jumps each, and perform 5–6 sets of exercises. The speed of jumping should be maintained once a second. In the training of the 20-meter single-leg jump, athletes should complete the training at the fastest speed and the maximum stride, control the balance and jumping rhythm of the body, and exchange feet for 10 sets each [13].

Sports is the last stage in sports training, the final finish of sports. Athletes need to maintain maximum speed and quickly hit the line. The requirements for the athlete to finish running are similar to those for running on the way. However, since athletes consume a lot of physical strength in the previous running stage, some techniques can be used to help athletes maintain their maximum speed when running at the finish line. When athletes are 15–20 meters away from the finish line, their upper body should lean forward and their center of gravity should move forward, which can increase the power of the back-push of the calf and at the same time increase the swing amplitude and step length of the arms, and always maintain the same cadence as the previous running stage [14]. In the sports running stage, athletes are required to have strong physical endurance and strength to support athletes rushing to the finish line [15]. Therefore, it is very necessary to strengthen the training of strength and endurance, and fast hopping is an efficient training method to strengthen the strength and endurance of athletes. During training, athletes can be trained by formulating rapid single-leg hops of different meters or by performing 50-100-meter mixed single-leg jumps, step jumps, and single-leg hop exchanges. Using this training method can increase the physical strength and endurance of athletes, promote the development of various comprehensive levels of athletes, and then fully demonstrate their own strength in sports training [16].

This paper combines the accurate recognition method of video image fuzzy features to accurately identify the sports process to explore the movement characteristics of athletes on the sports stage, which provides a reference for subsequent training and competition.

2. System Structure Design

2.1. Logic Design in FPGA. FPGA is the core device of the digital sports video recognition system, and the main digital logic functions of the spectrometer are implemented inside the FPGA. FPGA is divided by function and consists of the following parts:

(1) Data cache module

(2) Case storage module

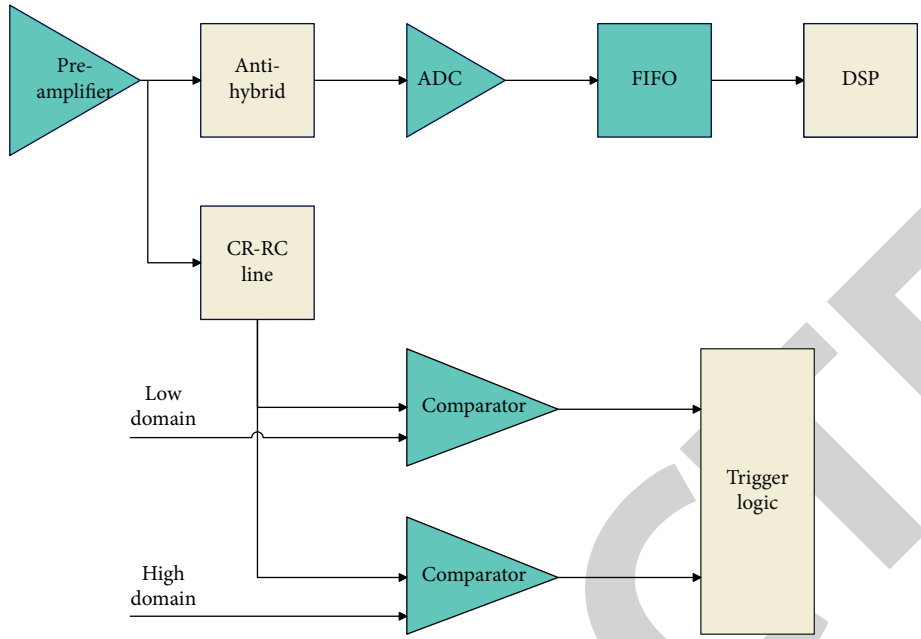

Figure 1: Schematic diagram of the traditional analog trigger circuit.

(3) Trigger module

(4) Digital filtering module (including shaping filtering and FIR low-pass filtering)

(5) Data processing module (including baseline elimination and peak finding)

(6) USB interface module

The digital sports video recognition system adopts the case-based operation mode. Each trigger corresponds to a good case. The function of the case storage module is to store the complete information of a good case. When the trigger signal is generated, the data in the data buffer is transferred to the instance storage module. The case storage module is also implemented with FIFO, and the length of the FIFO is the time length of the baseline plus the length of the shaping time of the pulse signal, which is determined by the type of the pulse signal generated by the detector. When the case storage FIFO is full, a full signal is generated and sent to the trigger module and the digital filter module, respectively. The function is to shield the trigger signal and notify the digital filter module to accept data for digital filtering. After filtering, the signal is reset, and the time in this paper is 6.4us.

2.2. Trigger Module. The sports video recognition system based on the case operation mode selects cases by triggering the system. The function of the trigger system is based on the voltage information sent by the detector, synthesizing the preset selection conditions of the physical case, realizing the response to the good case, and giving the corresponding trigger judgment. The data acquisition system selects and collects the case information of the electronics system according to the selection result of the trigger system and performs subsequent processing and data analysis on the useful data. The traditional sports video recognition system adopts the method of analog trigger selection, and its realization method is shown in Figure 1.

The signal output by the detector is divided into two channels, one channel enters the ADC for sampling through the antialiasing filter, and the other channel is used for trigger selection. The voltage signal output by the preamp is shaped by a simple CR-RC circuit and then enters a dual threshold comparator. When the signal amplitude is higher than the low threshold and lower than the high threshold, the trigger judgment logic generates a trigger signal to the case storage module. The information of the current trigger case stored in the case storage module is sent to the following digital signal processing device for subsequent processing and data analysis.

In order to set up a flexible and variable trigger system for different detector output pulse signals without changing the analog circuit, we adopted the all-digital trigger method in the digital sports video recognition system. The data flow input from ADC to FPGA is divided into two channels, one of which enters the digital trigger module, and each input voltage value is compared with the set low threshold trigger value. When the input value is greater than the low threshold trigger value, the trigger logic generates a high-level signal to notify the buffer module to transmit data to the case storage module. When the input value is higher than the high-threshold trigger value, the current case is judged as a bad case generated by accumulation, and the case is masked. In this paper, the ADC input overrange is used as the judgment standard for bad cases; that is, when the highest bit of the ADC output signal is "1" (the output level of the OTR pin is "1"), the case is discarded. When the case storage FIFO is full, the trigger signal is shielded, and even if a good case occurs, the trigger module will not respond. The trigger signal is turned on again only after the current good case has been processed by digital filtering and peak-seeking. This

requires the processing speed of the digital filtering and data processing modules to be as fast as possible to reduce the loss of good cases.

2.3. Digital Filter Module. The spectrum of the output signal of the charge-sensitive preamplifier is different from the power spectral density of the noise, and a suitable filtering system can be selected to maximize the signal-to-noise ratio to achieve the best filtering. The digital filtering module of the digital sports video recognition system is divided into two parts, one is the Gaussian filter for pulse shaping, and the other is the FIR low-pass filter for filtering noise. In the following, we introduce the two parts of the digital filtering module separately.

If the filter circuit is a linear system, its impulse response is $h(t)$, the frequency domain transduction coefficient is $H(\omega)$, and the output signal $V_0(t)$ and the output noise power spectral density $S_0(\omega)$ are obtained after the signal $V_i(t)$ and the noise power spectral density $S_i(\omega)$ are input, respectively [17]:

$$V_0(t) = \frac{1}{2\pi}\int_{-\infty}^{\infty} H(\omega)V_i(\omega)e^{j\omega t}d\omega, \tag{1}$$

$$S_0(\omega) = |H(\omega)|^2 S_i(\omega), \tag{2}$$

where $V_i(\omega)$ is the spectrum of $V_i(t)$. The magnitude of $V_0(t)$ reaching at $t = t_m$ is

$$V_{0m} = \frac{1}{2\pi}\int_{-\infty}^{\infty} V_i(\omega)H(\omega)e^{j\omega t_m}d\omega. \tag{3}$$

The mean square of the output noise is

$$V_n^2 = \frac{1}{2\pi}\int_{-\infty}^{\infty} |H(\omega)|^2 S_i(\omega)d\omega. \tag{4}$$

Then, there is a squared signal-to-noise ratio:

$$\eta^2 = \frac{\left|\int_{-\infty}^{\infty} \omega H(\omega)V_i(\omega)e^{j\omega t_m}d\omega\right|^2}{2\pi\int_{-\infty}^{\infty}|H(\omega)|^2 S_i(\omega)d\omega}. \tag{5}$$

To maximize η^2, it must satisfy

$$H(\omega) = K\frac{V_i^*(\omega)}{S_i(\omega)}e^{-j\omega t_m}. \tag{6}$$

We know that the input signal and noise spectral densities of the charge-sensing amplifier are

$$V_i(t) = \frac{Q}{C_f}u(t), \tag{7}$$

$$S_i(\omega) = \left(a^2 + \frac{b^2}{\omega^2} + \frac{C}{\omega}\right). \tag{8}$$

We assume that C is small, ignore it, and set $\omega_c = b/a$, which is called the corner frequency, and $\tau_c = 1/\omega_c$ is called the corner time:

$$S_i(\omega) = a^2\left(1 + \frac{1}{(\omega\tau_c)^2}\right). \tag{9}$$

After calculation, in

$$V_0(t) = \frac{Q}{2C_f}e^{-|t-t_m|/\tau_c}, \tag{10}$$

η reaches a maximum. At this time, the signal-to-noise ratio is

$$\eta_\infty = \frac{Q}{C_f\sqrt{2\pi b}} = \frac{Q}{\sqrt{2\pi a_i bc}}, \tag{11}$$

a_i is proportional to C_Σ^2, which can be written as [18]

$$a_i^2 = a_s C_\Sigma^2. \tag{12}$$

And then

$$\eta_\infty = \frac{Q}{\sqrt{2\pi a_s b_i C_\sum}}, \tag{13}$$

η_∞ is proportional to Q and inversely proportional to the square root of a_s, b_i, and $C_\sum$. This output signal is called an infinite spike pulse. Obviously, in order to get an output of this shape, it is required to generate an input at $t = 0$ and an output at $t < 0$, which is physically impossible unless t_m is required to be delayed to infinity. Nonetheless, it can be used as a standard against which other filters are compared.

In practical applications, we use the first-differential multi-integration filter shown in Figure 2 to achieve it.

Among them, $V_i(t)$ and $S_i(\omega)$ are the output signal and output noise power spectral density of the charge-sensitive amplifier. The figure shows the first-order differential and m-level integrator circuits, and their time constants RC are the same.

$$V_i(s) = L[V_i(t)] = L\left[\frac{Q}{C_f}u(t)\right] = \frac{Q}{SC_f}, \tag{14}$$

$$H(S) = \frac{\tau S}{(1+\tau S)^{m+1}}, \tag{15}$$

$$H(\omega) = \frac{j\omega t}{(1+j\omega t)^{m+1}}, \tag{16}$$

$$V_0(t) = L^{-1}[V_i(s)H(s)] = \frac{Q}{C_f}\cdot\frac{1}{m_i}\left(\frac{t}{\tau}\right)^m e^{-t/\tau}. \tag{17}$$

Among them, L[ ] and L^{-1} are the expressions of Laplace transform and inverse transform, respectively. It peaks at $t = m\tau$.

$$V_{0m} = \frac{Q}{C_f}\cdot\frac{m^m}{me^m}. \tag{18}$$

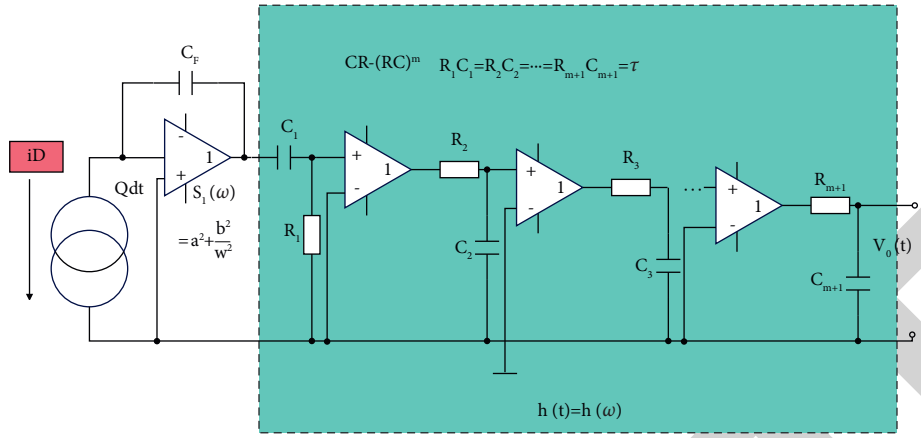

Figure 2: Implementation of the $CR-(RC)^m$ filter.

The waveforms of the $V_0(t)$ waveform at $m = 1, 2, 3$, and 4 are shown in Figure 3.

When m->∞, $V_0(t)$ tends to the shape of a Gaussian distribution function. The mean square value of noise at the output is

$$\begin{aligned}\overline{V_n^2} &= \int_0^\infty |H(\omega)|^2 S_i(\omega)d\omega \\ &= \int_0^\infty |H(\omega)|^2\left(a^2 + \frac{b^2}{\omega^2}\right)d\omega \\ &= a^2\int_0^\infty |H(\omega)|^2 d\omega + b^2\int_0^\infty \frac{|H(\omega)|^2}{\omega^2}d\omega \\ &= \frac{\pi_{ai}^2}{\tau}I_a + \tau b_i^2 I_b. \end{aligned} \tag{19}$$

Among them,

$$I_a = \frac{1}{\pi C_f^2}\int_0^\infty |H(\omega\tau)|^2 d(\omega\tau), \tag{20}$$

$$I_b = \frac{1}{\pi C_f^2}\int_0^\infty \frac{|H(\omega\tau)|^2}{(\omega\tau)^2}d(\omega\tau). \tag{21}$$

These two parameters will have nothing to do with the value of τ. When $\tau = \tau_c\sqrt{I_a/I_b}$ is taken, V_n^2 can be minimized, which can be obtained by calculation.

$$I_a = \frac{(2m-3)!!}{2C_f^2(2m)!!}, \tag{22}$$

$$I_b = (2m-1)I_a. \tag{23}$$

Among them, $(2m-3)!! = (2m-3)(2m-5)\cdots\cdots\times 3\times 1$, $(2m)!! = 2m(2m-2)(2m-4)\cdots\cdots\times 4\times 2$ When $\tau = \tau_c/\sqrt{2m-1}$, the optimal filter is obtained, and its inferior coefficient is

$$F = \frac{m!e^m}{m^m}(2m-1)^{1/4}\left[\frac{2m-3!!}{2(2m)!!}\right]^{1/2}. \tag{24}$$

It is best when $m = 1$, $\tau = \tau_c$, and $F = 1.359$.It is optimal when $m = 4$, $\tau = 0.378\tau_c$, and $F = 1.16$.When $m \longrightarrow \infty$, $F = 1.12$.

When $m \longrightarrow \infty$, the output waveform is Gaussian. When $m \geq 4$, the output waveform is close to a Gaussian shape, and we call it quasi-Gaussian filtering.

With the pulse signal input from the detector, after pole-zero cancellation and antialiasing, the rising edge becomes about 0.4s, and the falling edge becomes about 2.4us. After ADC sampling, it enters the digital filtering module of FPGA. The simulated waveforms before and after filtering are shown in Figure 4. The pulse signal amplitude is normalized in the figure.

The pulse signal is Gaussian shaped and then enters the FIR low-pass filter. After the output signal of the charge-sensitive preamplifier is shaped, its power is concentrated in the low-frequency region, and the influence of noise exists in the whole frequency domain. Therefore, using an FIR low-pass filter to filter out the noise in the high-frequency part can improve the signal-to-noise ratio. Since there is a ripple in the passband of the digital filter, it affects the performance of the filter. Therefore, we use the minimum ripple method to design the FIR filter.

We assume that the ideal FIR filter amplitude characteristic is $H_d(\omega)$, the amplitude characteristic of the actually designed filter is $H_s(\omega)$, and its weighted error $E(\omega)$ is expressed by the following formula:

$$E(\omega) = W(\omega)\left[H_d(\omega) - H_g(\omega)\right]. \tag{25}$$

Among them, $W(\omega)$ is the error weighting function, which is designed according to the different approximation accuracy required by the passband or stopband. To design an FIR filter with a linear phase, its unit impulse response $h(n)$ must satisfy certain conditions, and it is assumed that $h(n) = h(n-N-1)$, N = odd case. Then, there are

$$H\left(e^{j\omega}\right) = e^{-jN-1/2\omega}H_g(\omega). \tag{26}$$

Among them,

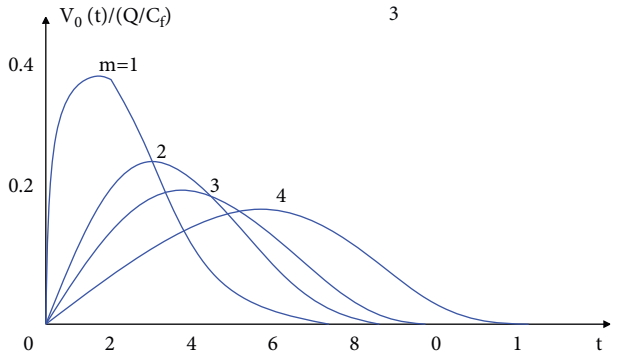

Figure 3: Gaussian-shaped waveform.

$$H_g(\omega) = \sum_{n=0}^{\frac{1}{2}(N-1)} \widetilde{a(n)} \cos \omega n. \tag{27}$$

When $M = (N-1)/2$ is substituted into formula 25, we get

$$E(\omega) = W(\omega)\left[H_d(\omega) - \sum_{n=0}^{M} \widetilde{a(n)} \cos \omega n\right]. \tag{28}$$

The best consistent approximation problem is to choose $M+1$ coefficients $\widetilde{a(n)}$ so that the maximum value of the weighted error $E(\omega)$ is the smallest, namely:

$$\min\left[\max_{\omega \in A} |E(\omega)|\right]. \tag{29}$$

In the formula, A represents the frequency band under study, which here refers to the passband or stopband. From formula 28, it can be seen that this is a problem of approximating a continuous function by the M-degree polynomial according to the above-mentioned criterion.

Chebyshev's theory points out that this polynomial exists and is unique and points out that the method for constructing this polynomial is the "interleaved point set theorem". The theorem states that the necessary and sufficient conditions for the best consistent approximation are as follows: $E(\omega)$ presents at least $M+2$ "staggers" on A such that

$$E(\omega_i) = E(\omega_{i+1}), \left|E(\omega_i)\right| = \max_{\omega \in A} |E(\omega)|. \tag{30}$$

Among them, $\omega_0 < \omega_1 < \cdots < \omega_{M+1}, \quad \omega \in A$. The filter passband or stopband designed according to this criterion has the property of minimum ripple.

It is assumed that what needs to be designed is a linear phase low-pass filter. If the frequency of $M+2$ interleaving points on A is known: $\omega_0, \omega_1, \ldots, \omega_{M+1}$, according to formula 28 and the interleaving point group criterion, it can be written as

$$W(\omega_k)\left[H_d(\omega_k) - \sum_{n=0}^{M} \widetilde{a(n)} \cos n\omega_k\right] = (-1)^k \rho. \tag{31}$$

Among them,

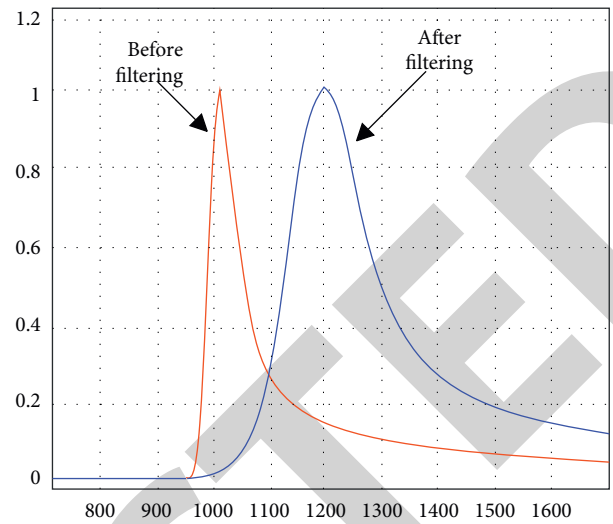

Figure 4: Gaussian shaping filter simulation.

$$\rho = \max|E(\omega)|, k = 0, 1, 2, \cdots M+1. \tag{32}$$

By writing Equation 32 in matrix form and solving it, $\widetilde{a(n)}$, $n = 0, 1, 2, \ldots$, M, and the maximum absolute value ρ of the weighted error can be uniquely obtained. From $\widetilde{a(n)}$, $h(n)$ of the filter can be found. In fact, the frequency $\omega_0, \omega_1, \ldots, \omega_M$ of these staggered point groups is unknown, and it is difficult to solve Equation (32). In numerical analysis, we often use the Remeg algorithm to solve it.

In the Remeg algorithm, the known condition is N, ω_p, ω_s, while δ_1, δ_2 are variables and can be optimally determined in an iterative process. In addition, if ω_p, ω_s are specified as the extremum frequency, at most $M+3$ extremum frequencies will appear. Therefore, using the staggered point group criterion, $M+2$ are needed, and only the frequency points with small errors in $\omega = 0$ and π need to be removed, and $M+2$ staggered point group frequencies are still selected.

The steps of the Remeg algorithm (Figure 5) are as follows:

(1) The algorithm takes $M+2$ frequencies $\omega_0, \omega_1, \ldots, \omega_{M+1}$ at equal intervals in the frequency domain as the initial value of the staggered point group. From,

$$H_g(\omega) = \sum_{n=0}^{M} \widetilde{a(n)} \cos \omega n, \tag{33}$$

the algorithm converts the multiplication of the cosine of the formula into the polynomial form of the cosine, namely:

$$\cos \omega n = \sum_{m=0}^{n} a_{mn} (\cos \omega)^m, \quad 0 \le \omega \le \pi. \tag{34}$$

The coefficient a_{mn} can be found in the relevant mathematics manual. Therefore,

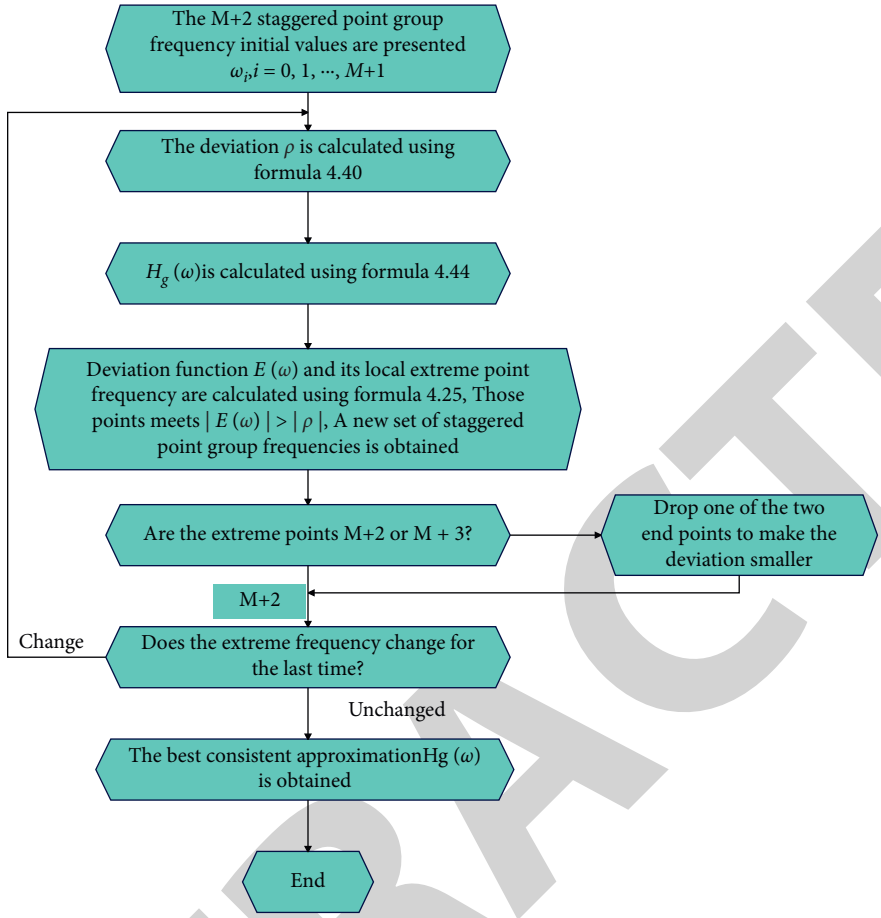

Figure 5: Flowchart of Remeg algorithm.

$$H_g(\omega) = \sum_{n=0}^{M} \widetilde{a(n)} \left[\sum_{m=0}^{n} a_{mn} (\cos\omega)^m \right] = \sum_{n=0}^{M} a(n) (\cos\omega)^n. \tag{35}$$

Among them, $a(n)$ is the result of combining the coefficients of the same power terms of $(\cos\omega)^n$.

Substituting the above formula into Equation 32, we get

$$W(\omega_k) \left[H_d(\omega_k) - \sum_{n=0}^{M} a(n) \cos^n \omega_k \right] = (-1)^k \rho. \tag{36}$$

Among them,

$$\rho = \max|E(\omega)|, \quad \underset{\omega \in A}{k = 0, 1, 2, \ldots M+1}. \tag{37}$$

The algorithm substitutes $M+2$ frequencies $\omega_0, \omega_1, \ldots, \omega_{M+1}$ as the initial value of the staggered point group into 33 and writes it in matrix form as

$$\begin{bmatrix} 1 & \cos\omega_0 & \cos^2\omega_0 & \cdots & \cos^M\omega_0 & \frac{1}{W(\omega_0)} \\ 1 & \cos\omega_1 & \cos^2\omega_1 & \cdots & \cos^M\omega_1 & \frac{-1}{W(\omega_1)} \\ 1 & \cos\omega_2 & \cos^2\omega_2 & \cdots & \cos^M\omega_2 & \frac{1}{W(\omega_2)} \\ \vdots & \vdots & \vdots & \vdots & \vdots & \vdots \\ 1 & \cos\omega_{M+1} & \cos^2\omega_{M+1} & \cdots & \cos^M\omega_{M+1} & \frac{(-1)^{M+1}}{W(\omega_{M+1})} \end{bmatrix} \begin{bmatrix} a(0) \\ a(1) \\ a(2) \\ \vdots \\ a(M) \\ \rho \end{bmatrix} = \begin{bmatrix} H_d(\omega_0) \\ H_d(\omega_1) \\ H_d(\omega_2) \\ \vdots \\ H_d(\omega_M) \\ H_d(\omega_{M+1}) \end{bmatrix}. \tag{38}$$

Then,

$$\rho = \frac{\sum_{k=0}^{M+1} H_d(\omega_k) A_{kM+2}}{\Delta}. \tag{39}$$

Among them, A_{ij} is the algebraic cofactor of a_{ij} in the determinant Δ.The determinant is

$$\Delta = \begin{vmatrix} 1 & \cos\omega_0 & \cos^2\omega_0 & \cdots & \cos^M\omega_0 & \frac{1}{W(\omega_0)} \\ 1 & \cos\omega_1 & \cos^2\omega_1 & \cdots & \cos^M\omega_1 & \frac{-1}{W(\omega_1)} \\ 1 & \cos\omega_2 & \cos^2\omega_2 & \cdots & \cos^M\omega_2 & \frac{1}{W(\omega_2)} \\ \vdots & \vdots & \vdots & \vdots & \vdots & \vdots \\ 1 & \cos\omega_{M+1} & \cos^2\omega_{M+1} & \cdots & \cos^M\omega_{M+1} & \frac{(-1)^{M+1}}{W(\omega_{M+1})} \end{vmatrix}. \tag{40}$$

Using the properties of the Vandermonde determinant again, the value of ρ can be obtained:

$$\rho = \frac{\sum_{k=0}^{M+1} a_k H_d(\omega_k)}{\sum_{k=0}^{M+1} (-1)^k a_k / W(\omega_k)}. \tag{41}$$

Among them,

$$a_k = (-1)^k \prod_{i=0, i\neq k}^{M+1} \frac{1}{\cos\omega_i - \cos\omega_k}. \tag{42}$$

Generally, the initial value ω_i is not the optimal extreme frequency, and ρ is not the optimal estimation error; it is the deviation from the initial value.

After ρ is calculated, the $H_g(\omega)$ value C_k at $M+1$ extreme frequency $\omega_0, \omega_1, \ldots, \omega_M$ can be determined, namely:

$$C_k = H_d(\omega_k) - (-1)^k \frac{\rho}{W(\omega_k)}, \quad k = 0, 1, \ldots M. \tag{43}$$

Then, using the Lagrangian interpolation formula in barycentric form, $H_g(\omega)$ is obtained, namely:

$$H_g(\omega) = \frac{\sum_{k=0}^{M} \beta_k / \cos\omega - \cos\omega_k C_k}{\sum_{k=0}^{M} \beta_k / \cos\omega - \cos\omega_k}. \tag{44}$$

In the formula,

$$\beta_k = (-1)^k \prod_{i=0, i\neq k}^{M} \frac{1}{\cos\omega_i - \cos\omega_k}. \tag{45}$$

By substituting $H_g(\omega)$ into formula 25, the error function is obtained.

$$E(\omega) = W(\omega)\left[H_d(\omega) - H_g(\omega)\right]. \tag{46}$$

If there is $|E(\omega)| \le |\rho|$ for all frequencies, ρ is the extreme value of the ripple, and the frequency $\omega_0, \omega_1, \ldots, \omega_{M+1}$ is the frequency of the staggered point group. Generally, the position of the first estimation will not be exactly the staggered point group but may be $|E(\omega)| > |\rho|$ at some frequencies, indicating that some points in the initial staggered point group need to be exchanged to form a new set of staggered point groups.

(2) For each point in the last determined $\omega_0, \omega_1, \ldots, \omega_{M+1}$, whether there is a certain frequency $|E(\omega)| > |\rho|$ in its vicinity is checked.2. If there is, the algorithm finds the local extreme point near the point and replaces the original point with this point. After all $M+2$ points have been checked, the algorithm obtains a new staggered point group

$\omega_0, \omega_1, \ldots, \omega_{M+1}$ and uses equations 25, 39, and 45 to find ρ , $H_g(\omega)$, and $E(\omega)$ again, so the algorithm completes an iteration and also completes an exchange of staggered point groups.

(3) Using the same method as the second step, the algorithm uses the point of $|E(\omega)| > |\rho|$ at each frequency as a new local extreme point, so as to obtain a new set of interleaved point groups. The algorithm repeats the above steps $\rho$and finally converges to its own upper limit, at which time $H_g(\omega)$ is best consistent with $H_d(\omega)$. If the algorithm iterates again, the peak value of the error curve $E(\omega)$ will not be greater than $|\rho|$, and the iteration ends. From the last set of staggered point groups, $H_g(\omega)$ is calculated according to formula 45, and $h(n)$ is calculated from $H_g(\omega)$.

While MATLAB software provides a large number of digital filtering functions, the FDATool toolbox is also developed. FDATool (Filter Design and Analysis Tool) is a filter design and analysis tool dedicated to the MATLAB signal processing toolbox. It is simple and flexible to operate and provides us with a variety of methods to design FIR and IR filters. FDATool also provides a high-quality graphical interface; we can choose the digital filter we need by setting parameters such as response type, design method, filter order, and cutoff frequency. Moreover, we can analyze the time-domain and frequency domain properties of the filter while setting up the digital filter.

Because the FIR system is not as easy to quantitatively obtain better passband and group band attenuation characteristics as the IIR system. In order to obtain better attenuation characteristics, the filter order is generally required to be higher. The order of the extralarge filter can improve the spectral characteristics, but for the FIR system, the increase of the order N will also increase the quantization noise caused by the finite word length effect. Therefore, for different detector signals, filters of appropriate order should be used for digital filtering.

We take a Gaussian pulse signal polluted by Gaussian white noise as an example to analyze the filtering effect of digital filters of different orders and types.

We assume that the Gaussian pulse amplitude is 1, the signal duration is 6us, and the signal waveform is shown in Figure 6.

Its frequency domain analysis is shown in Figure 7.

The ability of high-order digital filters to suppress noise is significantly better than that of low-order digital filters. When the selected digital filter order is the same, when the signal-to-noise ratio of the original signal is low, the filter with a low cutoff frequency is better than the filter with a high cutoff frequency. However, when the signal-to-noise ratio of the original signal is high when the filter is selected with a high cutoff frequency, the signal-to-noise ratio can be better improved. The signal-to-noise ratio of the original signal is 20db, the filter uses a 64-order Hamming window, and when the cutoff frequency is 1M, the waveform comparison before and after

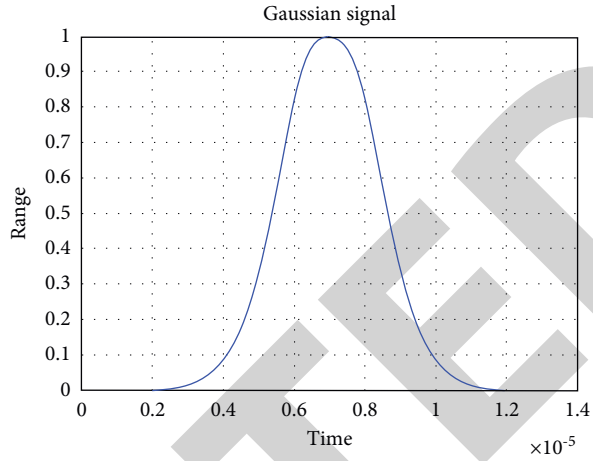

Figure 6: Gaussian signal.

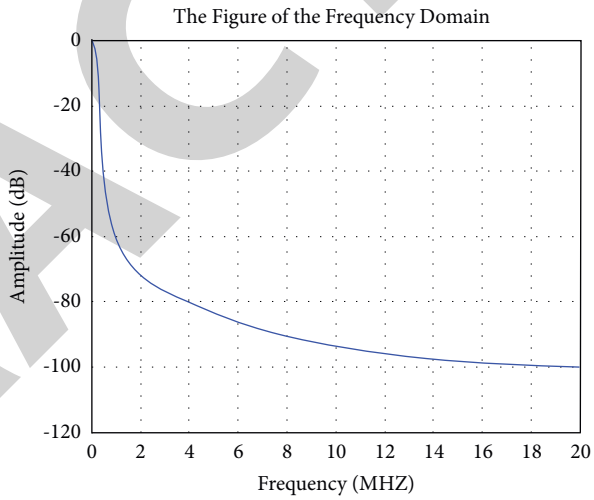

Figure 7: Gaussian signal frequency domain analysis.

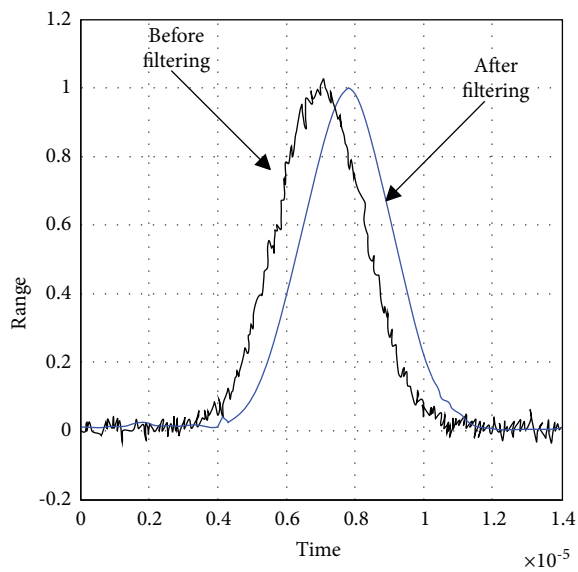

Figure 8: Simulation diagram of FIR digital filtering.

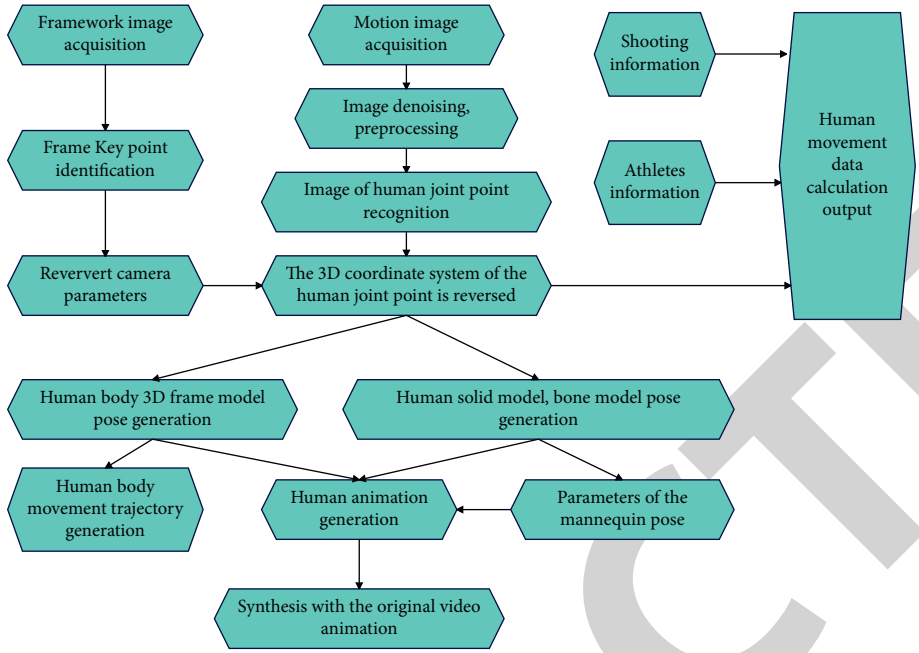

Figure 9: System workflow.

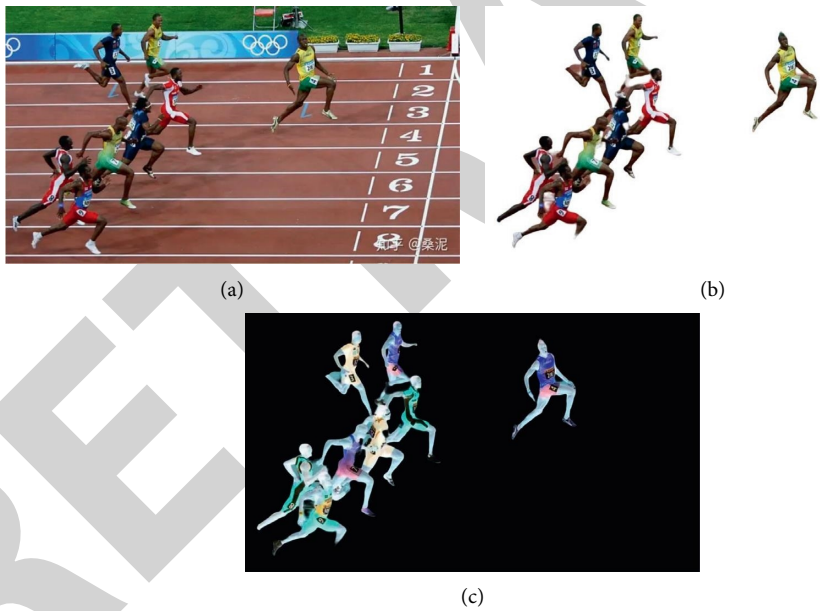

(a) (b)

(c)

Figure 10: Example of accurate recognition of local fuzzy features in sports video images.(a) Original video image. (b) Background removal. (c) Feature recognition.

filtering is shown in Figure 8. From the figure, we can clearly see that the noise suppression effect of the filter is very obvious.

3. Accurate Recognition System of Local Fuzzy Features in Sports Video Images

The determination of human kinematic parameters is the core content of sports technology diagnosis. The main instrument for testing human motion is a high-speed camera image analysis system. The system includes three parts: acquisition of moving images, image-to-number conversion, and data processing. The workflow of the system is shown in Figure 9.

Figure 10 shows an example of accurate recognition of local fuzzy features in sports video images.

The effect of the accurate recognition method of local fuzzy features in the sports video image is verified, and the recognition effect is counted, as shown in Table 1.

The above research verifies the effectiveness of the accurate recognition method of local fuzzy features in sports video images.

Table 1: Evaluation of the effect of accurate recognition of local fuzzy features in sports video images.

Num	Accurate identification	Num	Accurate identification	Num	Accurate identification
1	87.500	16	85.077	31	87.645
2	84.332	17	85.008	32	83.075
3	85.391	18	85.382	33	88.536
4	85.448	19	87.380	34	88.937
5	87.428	20	86.003	35	82.157
6	84.498	21	85.016	36	84.659
7	84.863	22	83.087	37	85.138
8	88.405	23	82.158	38	83.310
9	83.986	24	86.497	39	88.682
10	85.323	25	84.086	40	86.587
11	83.264	26	86.408	41	87.553
12	86.931	27	85.467	42	88.024
13	87.673	28	84.765	43	83.488
14	85.036	29	84.612	44	84.851
15	87.459	30	87.749	45	84.878

4. Conclusion

For sports training, the dash stage is reached after the end of the run. Especially in the dash, many students form a stride dash or jump dash, which affects the speed and movement skills of running. In fact, the trajectory of the body's center of gravity has changed a lot. The solution to this technique is to make the athlete maintain high speed and correct sports training technique, so that the running speed can be maintained or increased, and at the same time, the athlete should be reminded to gradually slow down after sports training and not stop suddenly, so as to avoid falling and injury. In this paper, the intelligent system is constructed by combining the method of intelligent video image partial fuzzy recognition. Moreover, this paper uses the accurate recognition method of video image fuzzy features to accurately identify the sports process to explore the movement characteristics of athletes on the sports stage. The effectiveness of the accurate recognition method of local fuzzy features in sports video images is verified through experimental research.

Data Availability

The labeled dataset used to support the findings of this study is available from the author upon request.

Conflicts of Interest

The author declares no conflicts of interest.

Acknowledgments

This work was supported by the Xinyang Agriculture and Forestry University.

References

[1] M. Li, Z. Zhou, and X. Liu, "Multi-person pose estimation using bounding box constraint and LSTM," *IEEE Transactions on Multimedia*, vol. 21, no. 10, pp. 2653–2663, 2019.

[2] J. Xu, K. Tasaka, and M. Yamaguchi, "Invited paper fast and accurate whole-body pose estimation in the wild and its applications," *ITE Transactions on Media Technology and Applications*, vol. 9, no. 1, pp. 63–70, 2021.

[3] G. Szűcs and B. Tamás, "Body part extraction and pose estimation method in rowing videos," *Journal of Computing and Information Technology*, vol. 26, no. 1, pp. 29–43, 2018.

[4] R. Gu, G. Wang, Z. Jiang, and J. N. Hwang, "Multi-person hierarchical 3d pose estimation in natural videos," *IEEE Transactions on Circuits and Systems for Video Technology*, vol. 30, no. 11, pp. 4245–4257, 2020.

[5] M. Nasr, R. Osama, H. Ayman, N. Mosaad, N. Ebrahim, and A. Mounir, "Realtime multi-person 2D pose estimation," *International Journal of Advanced Networking and Applications*, vol. 11, no. 06, pp. 4501–4508, 2020.

[6] N. T. Thành, L. V. Hùng, and P. T. Cong, "An evaluation of pose estimation in video of traditional martial arts presentation," *Journal of Research and Development on Information and Communication Technology*, vol. 2019, no. 2, pp. 114–126, 2019.

[7] I. Petrov, V. Shakhuro, and A. Konushin, "Deep probabilistic human pose estimation," *IET Computer Vision*, vol. 12, no. 5, pp. 578–585, 2018.

[8] W. McNally, A. Wong, and J. McPhee, "Action recognition using deep convolutional neural networks and compressed spatio-temporal pose encodings," *Journal of Computational Vision and Imaging Systems*, vol. 4, no. 1, p. 3, 2018.

[9] R. G. Díaz, F. Laamarti, and A. El Saddik, "DTcoach: your digital twin coach on the edge during COVID-19 and beyond," *IEEE Instrumentation and Measurement Magazine*, vol. 24, no. 6, pp. 22–28, 2021.

[10] A. Bakshi, D. Sheikh, Y. Ansari, C. Sharma, and H. Naik, "Pose estimate based yoga instructor," *International Journal of Recent Advances in Multidisciplinary Topics*, vol. 2, no. 2, pp. 70–73, 2021.

[11] S. L. Colyer, M. Evans, D. P. Cosker, and A. I. T. Salo, "A review of the evolution of vision-based motion analysis and the integration of advanced computer vision methods towards developing a markerless system," *Sports Medicine-Open*, vol. 4, no. 1, pp. 24–15, 2018.

[12] I. Sárándi, T. Linder, K. O. Arras, and B. Leibe, "Metrabs: metric-scale truncation-robust heatmaps for absolute 3d human pose estimation," *IEEE Transactions on Biometrics, Behavior, and Identity Science*, vol. 3, no. 1, pp. 16–30, 2021.

[13] A. Azhand, S. Rabe, S. Müller, I. Sattler, and A. Heimann-Steinert, "Algorithm based on one monocular video delivers highly valid and reliable gait parameters," *Scientific Reports*, vol. 11, no. 1, pp. 14065–14084, 2021.

[14] J. Xu and K. Tasaka, "[Papers] keep your eye on the ball: detection of kicking motions in multi-view 4K soccer videos," *ITE Transactions on Media Technology and Applications*, vol. 8, no. 2, pp. 81–88, 2020.

[15] Z. Li, J. Bao, T. Liu, and W. Jiacheng, "Judging the normativity of PAF based on TFN and NAN," *Journal of Shanghai Jiaotong University*, vol. 25, no. 5, pp. 569–577, 2020.

[16] J. Bhombe, A. Jethwa, A. Singh, and T. Nagarhalli, "Review of pose recognition systems," *VIVA-Tech International Journal for Research and Innovation*, vol. 1, no. 4, pp. 1–8, 2021.

[17] N. V. Dr P Prabhavathy, "The analysis of the impact of yoga on healthcare and conventional strategies for human pose recognition," *Turkish Journal of Computer and Mathematics Education (TURCOMAT)*, vol. 12, no. 6, pp. 1772–1783, 2021.

[18] J. J. Liu, J. Newman, and D. J. Lee, "Using artificial intelligence to provide visual feedback for golf swing training," *Electronic Imaging*, vol. 33, no. 6, pp. 3211–3216, 2021.